Catal Lett (2008) 125:90–96
DOI 10.1007/s10562-008-9519-0

Dehydrogenation of Ethylbenzene in the Presence of CO_2 over V Catalysts Supported on Nano-sized Alumina

Bin Xiang · Changlin Yu · Hengyong Xu · Wenzhao Li

Received: 13 February 2008 / Accepted: 8 May 2008 / Published online: 28 May 2008
© Springer Science+Business Media, LLC 2008

Abstract Nanocrystalline alumina was prepared and was employed as a support for vanadium catalysts. The catalysts were characterized by N_2 adsorption/desorption, X-ray diffraction, TPR, UV–Vis, NH_3-TPD, and CO_2-TPSR. The activity and selectivity of the catalysts in ethylbenzene dehydrogenation in the presence of CO_2 were compared with vanadium supported on commercial available alumina. The catalytic activity, selectivity, and stability were enhanced by the use of nanocrystalline alumina as catalyst supports. The superior performance of the present nano-crystalline alumina catalysts was attributed to the higher surface areas, higher vanadium dispersion, and higher stability of V^{5+} against reduction.

Keywords Ethylbenzene · Dehydrogenation · Carbon dioxide · Supported vanadium oxide catalyst · Nano-sized alumina

1 Introduction

Styrene is one of the most important monomer of synthetic polymers. Ethylbenzene (EB) dehydrogenation as a representative process for the production of styrene is performed on the promoted iron oxide catalysts in the presence of a large quantity of steam at high temperatures of 600–700 °C [1–5]. Since the current process is equilibrium limited and high energy consuming, there is a strong incentive for the development of new process and catalysts [6–9].

B. Xiang · C. Yu · H. Xu (✉) · W. Li
Dalian Institute of Chemical Physics, Chinese Academy of Sciences, Dalian 116023, Liaoning, China
e-mail: xuhy@dicp.ac.cn

The dehydrogenation of EB in the presence of CO_2 as an energy saving and environmentally friendly process has received much attention [10–21]. It is estimated that the energy required for producing per ton styrene in this process is 1.5–1.9 $\times$ 10^8 cal, compared with 1.5 $\times$ 10^9 cal in the current commercial process [10, 11]. The process could be effective in respect of utilization of carbon dioxide which is one of greenhouse gases causing global warning. High performance catalysts have been screened extensively and some new catalysts were reported [12–19]. Iron oxide-based catalysts supported on Al_2O_3 and active carbon (AC) [12, 13], vanadium oxide catalysts supported on Al_2O_3 [14–16], MgO [17], SBA-15 [18], and AC [19], catalysts obtained by thermal decomposition of hydrotalcite-like precursors [20], and ZrO_2 [21] catalysts exhibited high catalytic activity for EB dehydrogenation in the presence of CO_2. Among these catalysts, vanadia supported on alumina (VO_x/Al_2O_3) catalysts were more stable and exhibited reasonable activity [14–16]. However, the deactivation due to the coke deposition and the deep reduction of the surface vanadium species still restrains the practical utilization of VO_x/Al_2O_3 catalysts [14]. In this study, the nano-sized alumina-supported vanadium oxide catalysts which exhibit high stability in EB dehydrogenation in the presence of CO_2 catalysts were reported. The influence of the supports, nano-sized Al_2O_3, and commercial Al_2O_3, on the catalytic performance of vanadia catalysts in EB dehydrogenation reaction was discussed.

2 Experimental

2.1 Catalyst Preparation

Nano-sized alumina was prepared by a precipitation method. Aluminum nitrate [$Al(NO_3)_3$] and ammonium

carbonate [$(NH_4)_2CO_3$] with molar ratio of 1:3 were used as the starting materials. A solution of $Al(NO_3)_3$ was added to a solution of $(NH_4)_2CO_3$ containing polyethylene glycol and stirred for 1 h at 38 °C. The PH value of the solution of $(NH_4)_2CO_3$ was adjusted to about 9.0 by ammonia previously. The precipitate was aged in the mother liquor, removed, washed thoroughly with ethanol, and the obtained solid was dried at 120 °C for 12 h, and finally calcined at 600 °C for 3 h.

Vanadia supported on nano-sized alumina catalysts were prepared by impregnation of nano-sized alumina with NH_4VO_3 dissolved in oxalic acid solution. The excess water was then slowly evaporated on a water bath with continuous stirring. The residues thus obtained were dried in air at 120 °C for 12 h. After calcination at 550 °C for 3 h, the catalysts were cooled to room temperature, crushed, and sieved into granules of 60–80 mesh for the EB dehydrogenation reaction tests. Different samples are designated in the text as nV/Al_2O_3, where n is an integer corresponding to the nominal loading of vanadia on γ-Al_2O_3 as percentage by weight of V_2O_5. For comparison, vanadia catalysts supported on commercial γ-Al_2O_3 (S_{BET}: $\geq$250 m^2 g^{-1}), has also been prepared by the same procedure.

2.2 Catalyst Characterization

The BET surface areas of the alumina and alumina supported vanadia catalyst powders were measured by nitrogen physisorption at 77 K with a surface area analyzer, Quantachrome NOVA 4000. The catalyst samples were evacuated at 350 °C for 3 h before N_2 physisorption measurements. X-ray diffraction (XRD) experiments were performed on a Philips X'Pert Highscore powder diffractometer equipped with a monochromated Cu Kα radiation.

Diffuse reflectance UV–Vis spectra were obtained using MgO as a reference in a UV-240 spectrophotometer. Reflectance data were converted to absorption spectra. Considering that the nature of the supported vanadium is highly moisture sensitive [22, 23], to identify the exact vanadium environment, diffuse reflectance spectra in the UV–Vis region of samples were recorded in the dehydrated state. Prior to recording of the UV–Vis spectra, the samples were treated under dry air at 450 °C for 3 h.

Transmission electron microscopy (TEM) was recorded on a FEI TECNAI G^2 SPIRIT transmission electron microscope. The samples were prepared by dispersing the powder products in ethanol, which was then deposited and dried on a holey carbon film on a Cu grid.

Temperature-programmed reductions (TPR) experiments were carried out in a conventional setup equipped with a programmable temperature furnace. Each sample was pretreated by passing high-purity (99.9%) argon (20 mL/min) at 110 °C for 30 min and at 350 °C for 30 min. After cooling to ambient temperature, the argon flow was replaced by 5% H_2/Ar mixture. TPR experiments were performed under this atmosphere to 900 °C at a heating rate of 10 °C/min. The consumption of hydrogen was monitored with a thermal conductivity detector (TCD).

To investigate the acidity of catalyst, NH_3-TPD was performed on a chemisorption analyzer equipped with an on-line mass spectrometer (Omnisorp. Corp.). Samples (0.1 g) were placed into a quartz U-type reactor between two quartz wool plugs. The samples were treated by flowing dry argon (99.99%) at 300 °C for 1 h prior to adsorption of ammonia. Pure NH_3 was injected until adsorption saturation followed by purging with He for 3 h. The temperature was raised at a rate of 8 °C/min to 700 °C. The TPD process was monitored by the on-line mass spectroscope (Omnisorp. Corp.).

CO_2-TPSR was performed on a chemisorption analyzer equipped with an on-line mass spectrometer (Omnisorp. Corp.). The reacted catalyst (0.1 g) was placed into a quartz U-type reactor between two quartz wool plugs. The sample was treated by flowing dry argon (99.99%) at 300 °C for 1 h. Then, sample was saturated by a CO_2 pulse at room temperature. Before the run, the baseline was stabilized in dry argon (30 mL/min) at the same temperature for 3 h. The temperature was raised at a rate of 8 °C/min to 960 °C.

2.3 Catalytic Tests

Catalytic reactions were carried out in a quartz fixed-bed reactor at 550 °C under atmospheric pressure. About 0.2 g of catalyst was placed at the center of the reactor with quartz wool plugs. EB was introduced by a high-pressure syringe pump with a feed flow rate of 9.81 mmol/h. The molar ratio of CO_2 to EB was 10 and W/F was controlled at 9.26 g_{cat}h/mol (i.e., 101.9 g_{cat} h/mol_{EB}). The flow of CO_2 was controlled by a mass flow controller. Gaseous and liquid products were analyzed simultaneously by on-line GC (Shimadzu 14C): aromatic compounds were analyzed by a FID detector using stainless steel column packed with 2.5% DNP. Gaseous products were analyzed by a TCD detector using a packed carbon molecular sieve column. Turnover frequencies (TOFs) (mol_{EB} mol^{-1} $_V$ s^{-1}) were calculated from conversion values of EB (X_{EB}), with the use of vanadium contents of the samples.

3 Results and Discussion

3.1 Catalytic Results

The EB conversion, selectivity to styrene, TOFs for styrene formation, and styrene yield over the V-containing nano-sized catalysts in the presence of CO_2 were summarized in

Table 1 Dehydrogenation of EB in the presence of CO_2 on the supported vanadium oxide catalysts

Catalyst	EB conversion (%)	Selectivity (%)			Styrene yield (%)	TOF (μmol_{EB} mol^{-1} $_V$ s^{-1})
		Styrene	Benzene	Toluene		
5 V/nano-Al_2O_3	61.5	94.4	3.2	2.4	58.0	2.88
10 V/nano-Al_2O_3	67.0	93.5	3.1	3.4	61.7	1.53
15 V/nano-Al_2O_3	69.7	94.9	2.1	3.0	66.2	1.09
25 V/nano-Al_2O_3	73.7	96.2	1.5	2.4	70.8	0.70
30 V/nano-Al_2O_3	71.8	96.7	1.1	2.2	69.4	0.57

Reaction conditions: WHSV = 1.04, CO_2/EB = 10/1, time-on-stream = 2.5 h, temperature = 550 °C

Table 1. From this table, it can be seen that the conversion of EB increased with vanadia loading up to 25 wt% V_2O_5. The styrene selectivity of 96.2% and EB conversion of 73.7% could be achieved over the 25 V/nano-Al_2O_3 catalyst. With the further increase of vanadia loading, a slight decrease of EB conversion appeared. As shown in Table 1, the TOFs for styrene formation decrease with the vanadium loading. But the optimal vanadia loading can contribute to the high yield of styrene. Figure 1 gives the catalytic performance comparison of vanadia dispersed on the nano-sized Al_2O_3 and commercial Al_2O_3 at the same V_2O_5 loading level of 5 wt%. From Fig. 1, it can be seen that the 5 V/nano-Al_2O_3 catalyst exhibited much higher stability than that of 5 V/com-Al_2O_3. For 5 V/com-Al_2O_3, the yield of styrene decreased from 56.6 to 49.0% after 4 h reaction, while no significant decrease was observed with 5 V/nano-Al_2O_3 catalyst.

3.2 Catalyst Characterization

The BET surface areas (S_{BET}) of vanadium oxide catalysts supported on nano-sized Al_2O_3 and commercial Al_2O_3 are shown in Table 2. The value of S_{BET} of the nano-sized Al_2O_3 was found to be 275 m^2 g^{-1}. A consistently decreasing trend is observed with increasing V_2O_5 loading on nano-sized alumina. This is primarily due to the penetration of vanadia into the pores of Al_2O_3. The S_{BET} value of the com-Al_2O_3 was 250 m^2 g^{-1}. After loading V_2O_5, the BET surface area of 5 V/nano-Al_2O_3 was 270 m^2 g^{-1}, which is much higher than that of 5 V/com-Al_2O_3 (195 m^2 g^{-1}).

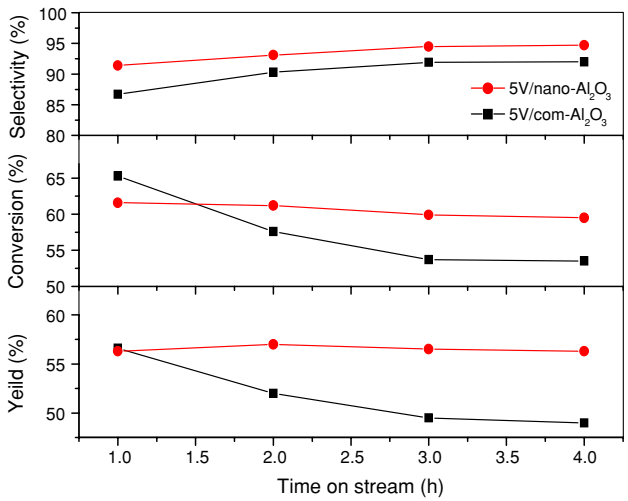

Fig. 1 The performance comparison of the catalysts in EB dehydrogenation at 550 °C

The XRD patterns of V_2O_5/nano-Al_2O_3 catalysts of various V_2O_5 loadings are shown in Fig. 2. Very sharp peaks at d = 1.4, 2.0, and 2.4 Å, which corresponds to γ-Al_2O_3 (JCPDS 10-0425), appears over the nano-Al_2O_3 support. The most intense peak of γ-Al_2O_3 (d = 1.40) was considered for the calculation of the averaged particle size of the alumina support with the Scherrer equation. The particle sizes were found to be around 8.7 nm for V/nano-Al_2O_3 catalysts and did not vary significantly with vanadia loading (shown in Table 2). The V_2O_5/nano-Al_2O_3 samples with V_2O_5 content above 15 wt% showed X-ray reflections at d = 2.9, 3.4, and 4.4 Å corresponding to crystalline V_2O_5 (JCPDS 9-387) and the intensity increased gradually with increase of vanadia loading. These results indicated that vanadia was high dispersed when the loading is below 15 wt%. Over the loading of 15 wt%, microcrystalline V_2O_5 phase appears.

Figure 3 shows the TEM images of 5 V/nano-Al_2O_3 (Fig. 3a) and 5 V/com-Al_2O_3 (Fig. 3b). It was found that the particles of 5 V/nano-Al_2O_3 catalysts were well dispersed and the particle size was less than 10 nm. The TEM image showed that the particles of 5 V/com-Al_2O_3 appeared to be more agglomerated than the 5 V/nano-Al_2O_3 sample. The 5 V/com-Al_2O_3 had both large separate spherical particles and flakes, which were formed by aggregation of their primary particles.

The TPR profiles of various supported vanadium oxide catalysts are shown in Fig. 4 and their main features are summarized in Table 2. The temperature of the maximum reduction peak (T_{max}) was 567 °C for 5 V/nano-Al_2O_3 (Fig. 4b). With the increase of vanadia content, up to 10 wt%, the T_{max} values shifted to lower temperature,

Table 2 Characteristics of the supported vanadium oxide catalysts

Sample	S_{BET} ($m^2\ g^{-1}$)	V_p ($cm^3\ g^{-1}$)	Particle size[a] (nm)	UV–Vis edge energy (eV)	H_2 TPR[b] T_{max1} (°C)
Nano-Al_2O_3	275	0.57	8.7	–	718
5 V/nano-Al_2O_3	270	0.52	8.7	2.70	569
15 V/nano-Al_2O_3	254	0.49	8.8	2.38	567
25 V/nano-Al_2O_3	206	0.43	9.6	2.25	590
30 V/nano-Al_2O_3	188	0.42	9.4	2.19	614
Com-Al_2O_3	250	–	–	–	758
5 V/com-Al_2O_3	195	0.44	10.7	2.63	552

[a] Calculated by Scherrer formula

[b] Temperature of the maximum hydrogen consumption (T_{max})

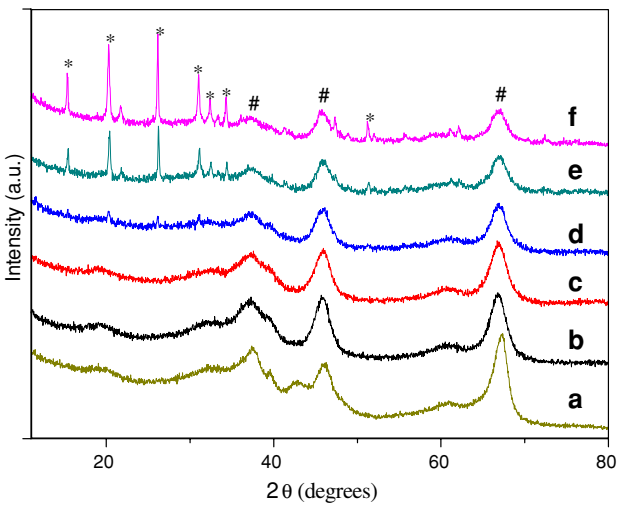

Fig. 2 XRD patterns of calcined nano-sized Al_2O_3 and V_2O_5/nano-Al_2O_3 catalysts (*, V_2O_5; #, Al_2O_3): (a) 5 V/com-Al_2O_3; (b) nano-Al_2O_3; (c) 5 V/nano-Al_2O_3; (d) 15 V/nano-Al_2O_3; (e) 25 V/nano-Al_2O_3. (**f**) 30 V/nano-Al_2O_3

around 556 °C (Fig. 4c). The appearance of easily reducible VO_x species in 10 V/nano-Al_2O_3 could be related to the results of the presence of polymeric vanadium species. The polymeric vanadium species are more easily to be reduced than the monomeric vanadium species, probably due to the weaker vanadium–oxygen bonds which can be easier detached by H_2. Similar behavior was described by earlier reports [7, 8]. In the sample, with V_2O_5 content above 10 wt%, the reduction peak becomes broader and shift to higher temperature. According to the previous studies on the reducibility of VO_x/Al_2O_3, the peak at higher temperature is attributed to the reduction of bulk-like V_2O_5 crystallites [7, 14, 22]. This is well in accordance with XRD results which show the presence of V_2O_5 crystallites for the samples with vanadium loading higher than 15 wt%. Both nano-sized Al_2O_3 Fig. 4a) and com-Al_2O_3 (Fig. 4 h) show a reduction peak at about 727 °C. The origin of the peak is not clearly known. The T_{max} of 5 V/nano-Al_2O_3 is 569 °C, which is higher than that of 5 V/com-Al_2O_3 (552 °C), indicating that VO_x species in the 5 V/com-AL_2O_3 are more easily to be reduced than those in the 5 V/nano-Al_2O_3. This suggests that the interactions

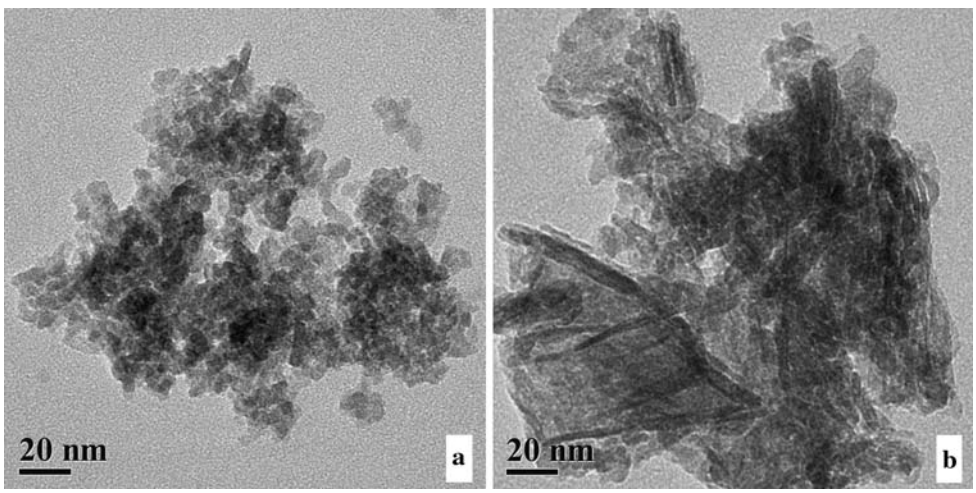

Fig. 3 TEM images of supported vanadium catalysts: (**a**) 5 V/nano-Al_2O_3; (**b**) 5 V/com-Al_2O_3

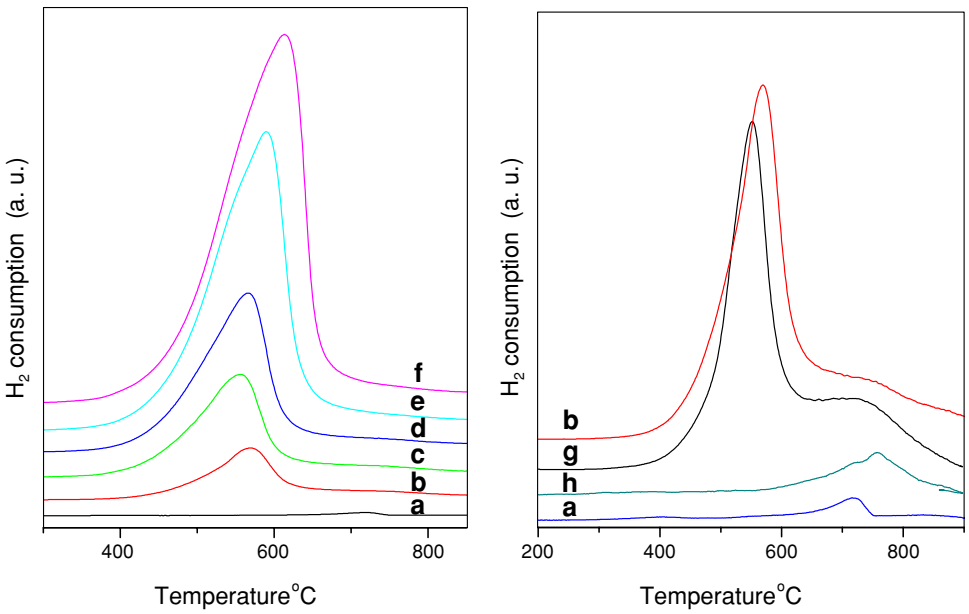

Fig. 4 H_2-TPR results of the alumina supported vanadium oxide catalysts: (a) nano-Al_2O_3; (b) 5 V/nano-Al_2O_3; (c) 10 V/nano-Al_2O_3; (d) 15 V/nano-Al_2O_3; (e) 25/nano-Al_2O_3; (f) 30 V/nano-Al_2O_3; (g) 5 V/com-Al_2O_3; (h) com-Al_2O_3

between active species and support over the nano-Al_2O_3 catalyst are stronger than those over common Al_2O_3. According to the previous report that the reduction of V^{5+} will cause the deactivation of vanadium catalysts [14], the interactions between active species and support over the nano-Al_2O_3 catalyst may be one of the important reasons for 5 V/nano-Al_2O_3 to exhibit more stable activity.

Figure 5 shows the diffuse reflectance UV–Vis spectra of calcined VO_x/Al_2O_3 samples after dehydration under dry air at 450 °C. A very broad band centered at ca. 300 nm is observed, corresponding to the isolated V sites in tetrahedral coordination and polymeric V–O–V species [22, 23]. As the vanadium content increases, a new feature at 450 nm appears for the samples with 25 wt% V_2O_5 loading, indicating the presence of "bulk-like" V_2O_5 crystallites due to a further polymerization of the V species [22, 23]. The edge energies determined from the position of the low energy rise in the UV–Vis spectrum have been used previously to characterize the domain sizes of VO_x in catalytic solids [22, 23]. The edge energies for the present series of catalysts were determined with Tauc's law from the intercept of a straight line fitted through the rise of the function $[F(R\alpha)hv]^2$ plotted versus hv, where $F(R\alpha)$ is a Kubelka–Munk function [24] and hv is the energy of the incident photon. The values obtained for the dehydrated catalysts are listed in Table 2. The edge energy is 2.70 eV for 5 V/nano-Al_2O_3, which decreases to 2.19 eV with increasing vanadia to 30 wt%. The decrease in edge energy with increasing vanadia content indicates that the size and polymerization of VO_x increased with increasing vanadia content. The edge energy is 2.63 eV for 5 V/com-Al_2O_3, which is lower than that of 5 V/nano-Al_2O_3. This indicates that the polymerization degree of the surface vanadia species of 5 V/com-Al_2O_3 is higher than that of 5 V/nano-Al_2O_3. The high dispersed vanadia species will promote the interactions between active species and support, and enhance the stability of catalyst.

To investigate the influence of acidity on the catalytic reactions, NH_3-TPD was performed and the results are shown in Fig. 6. It is seen that both of com-Al_2O_3 and nano-Al_2O_3 exhibited a NH_3 desorption peeks at 130 °C. For the vanadium-containing samples, the desorption peaks shifted to higher temperature, suggesting the formation of new type of acid sites. Moreover, the number of acid

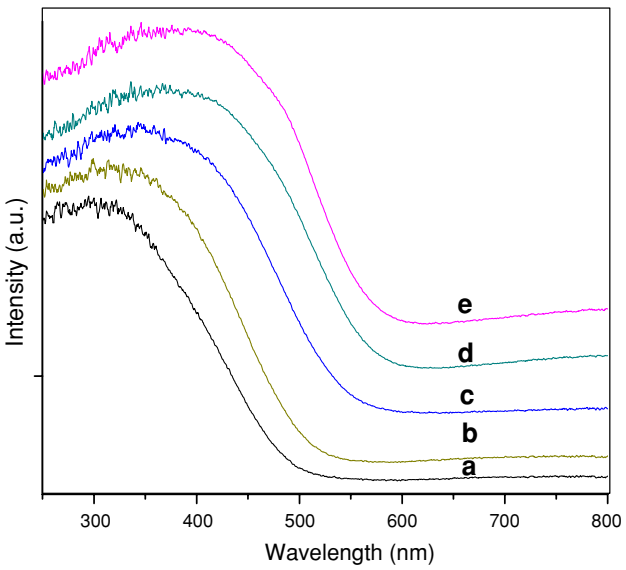

Fig. 5 UV–Vis spectra of calcined and dehydrated VOx/Al_2O_3 samples: (a) 5 V/nano-Al_2O_3; (b) 5 V/com-Al_2O_3; (c) 15 V/nano-Al_2O_3; (d) 25 V/nano-Al_2O_3; (e) 30 V/nano-Al_2O_3

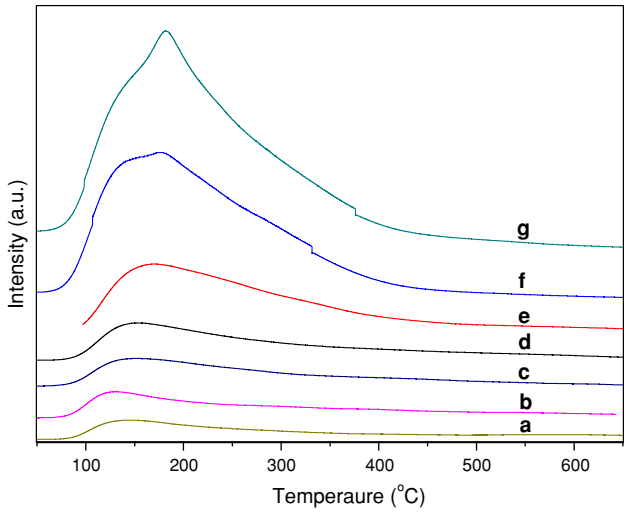

Fig. 6 NH_3-TPD results of the alumina supported vanadium oxide catalysts: (a) com-Al_2O_3; (b) nano-Al_2O_3; (b) 5 V/com-Al_2O_3; (d) 5 V/nano-Al_2O_3; (e) 15 V/nano-Al_2O_3; (f) 25/nano-Al_2O_3. (g) 30/nano-Al_2O_3

strength increases with increasing vanadia content for the vanadium-containing catalysts. 25 V/nano-Al_2O_3 and 30 V/nano-Al_2O_3 samples displayed a shoulder at 180 °C, indicating the formation of relatively stronger acid strength sites. The stronger acid site may be corresponded to the formation of bulk like V_2O_5, considering the results of UV–Vis and TPR.

To gain a further insight into the role of carbon dioxide in EB dehydrogenation over VO_x/nano-Al_2O_3 about the coke deposition, CO_2-TPSR of used 25 V/nano-Al_2O_3 was performed and the results are shown in Fig. 7. Mamedov and Corberan [25] reported that one of the main roles of CO_2 in the catalytic dehydrogenation process is the removal of the deposited coke. It is seen that CO and water were produced at temperature higher than 600 °C. This indicates that CO_2 can react with coke deposition at temperature higher than 600 °C. Chen et al. [14] have reported that coke deposited on VO_x/Al_2O_3 catalysts in the presence of CO_2 cannot be effectively suppressed by CO_2. CO_2 play the role of eliminating hydrogen produced during EB dehydrogenation and regaining the oxidation state (lattice oxygen) of reduced vanadium species.

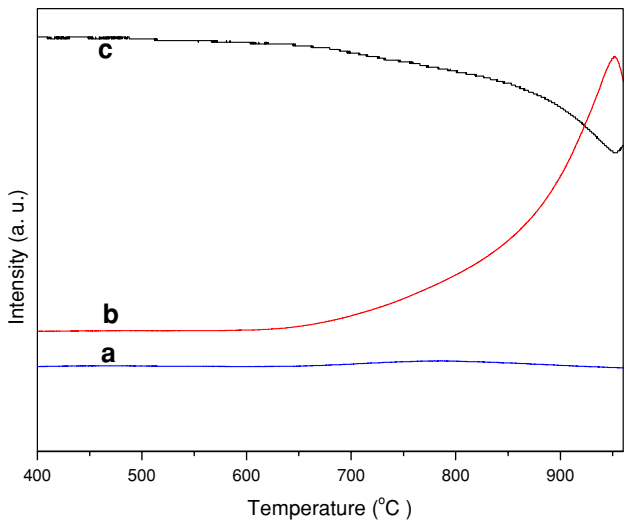

Fig. 7 CO_2-TPSR results of used 25 V/nano-Al_2O_3 catalyst: (a) H_2O signal (m/e = 18); (b) CO signal (m/e = 28); (c) CO_2 signal (m/e = 44)

4 Conclusions

The prepared nanocrystalline alumina as catalyst support shows superiority than the common alumina in the dehydrogenation of EB. Over the nanocrystalline alumina supported catalyst, the catalytic activity, selectivity, and stability were enhanced. An EB conversion of 73.7% with styrene selectivity of 96.2% was obtained on the 25 V/nano-Al_2O_3 at 550 °C. BET, XRD, UV–Vis, and TPR results indicate that the nano-Al_2O_3 supported vanadium catalysts possessed higher surface areas, higher vanadium dispersion, and higher stability of V^{5+} against reduction. All of these are considered to be responsible for the superior catalytic behavior of the V/nano-Al_2O_3 catalyst in the dehydrogenation of EB.

References

1. Kochloefl K (1997) In: Ertl G, Knozinger H (eds) Handbook of heterogeneous catalysis, vol 5. Wiley, Weinheim, p 2151
2. Peng F, Fu X, Yu H, Wang H (2007) Carbon 45:1
3. Muhler M, Schütze J, Wesemann M, Rayment T, Dent A, Schlögl R, Ertl G (1990) J Catal 126:339
4. Dulamiţă N, Măicăneanu A, Sayle DC, Stanca M, Crăciun R, Olea M, Afloroaei C, Fodor A (2005) Appl Catal A 287:9
5. Serafin I, Kotarba A, Grzywa M, Sojka Z, Bińczycka H, Kuśtrowski P (2006) J Catal 239:137
6. Sato S, Ohhara M, Sodesawa T, Nozaki F (1988) Appl Catal 37:207
7. Shiju NR, Anilkumar M, Mirajkar SP, Gopinath CS, Rao BS, Satyanarayana CV (2005) J Catal 230:484
8. Sun A, Qin Z, Wang J (2002) Catal Lett 79:33
9. Zhang J, Su DS, Zhang AH, Wang D, Schlögl R (2007) Angew Chem Int Ed 46:7319
10. Mimura N, Saito M (1999) Catal Lett 58:59
11. Mimura N, Saito M (2000) Catal Today 55:173
12. Saito M, Kimura H, Mimura N, Wu J, Murata K (2003) Appl Catal A 239:71
13. Badstube T, Papp H, Kustrowski P, Dziembaj R (1998) Catal Lett 55:169
14. Chen S, Qin Z, Xu X, Wang J (2006) Appl Catal A 302:185
15. Hong D, Vislovskiy VP, Hwang YK, Jhung SH, Chang J (2008) Catal Today 131:140
16. Sun A, Qin Z, Chen S, Wang J (2004) J Mol Catal A 210:189
17. Sakurai Y, Suzaki T, Nakagawa K, Ikenaga N, Aota H, Suzuki T (2002) J Catal 209:16

18. Liu BS, Rui G, Chang RZ, Au CT (2008) Appl Catal A 335:88
19. Sakurai Y, Suzaki T, Ikenaga N, Suzuki T (2000) Appl Catal A 192:281
20. Mimura N, Takahara I, Saito M, Sasaki Y, Murata K (2002) Catal Lett 78:125
21. Burri DR, Choi KM, Han Sajandi D, Jiang N, Burri A, Park S (2008) Catal Today 131:173
22. Liu Y, Cao Y, Yi N, Feng W, Dai W, Yan S, He H, Fan K (2004) J Catal 224:417
23. Baltes M, Cassiers K, Voort PV, Weckhuysen BM, Schoonheydt RA, Vansant EF (2001) J Catal 197:160
24. Di W, Hui W, Xiaobing F, Chueh W, Ravikovitch P, Lyubovsky M, Li C, Takeguchi T, Haller GL (1999) J Phys Chem B 103:2113
25. Mamedov EA, Corberan VC (1995) Appl Catal A 127:1